



**2<sup>nd</sup> International Conference on  
Ultrafine Grained and Nanostructured Materials  
Center of Excellence For High Performance Materials  
School of Metallurgy and Materials Engineering  
University College of Engineering, University of Tehran  
Tehran, Iran. 14-15 Nov. 2009**

**Reverse Precipitation Synthesis and Characterization of CeO<sub>2</sub> Nanopowder**

S. A. HASANZADEH-TABRIZI<sup>†</sup>

*Materials and Energy Research center  
Karaj, Tehran, Iran  
tabrizi1980@yahoo.com*

M. MAZAHERI

*Institute of Physics of Complex Matter, Swiss Federal Institute of Technology Lausanne (EPFL)  
1015 Lausanne, Switzerland  
mehdi.mazaheri@epfl.com*

M. AMINZARE

*Materials and Energy Research center  
Karaj, Tehran, Iran  
masoudaminzare@yahoo.com*

S. K. SADRNEZHAD

*Materials and Energy Research center  
Karaj, Tehran, Iran  
sadrneh@yahoo.com*

Received Day Month Day

Revised Day Month Day

In the present work, CeO<sub>2</sub> nanopowder was synthesized via a reverse precipitation method using CeCl<sub>3</sub>\*7H<sub>2</sub>O, NH<sub>4</sub>OH and Sodium dodecyl sulfate as raw materials. The effect of thermal treatment on the crystal growth, surface area and chemical bonds of the powder was discussed. The structural evolutions and morphological characteristics of the nanopowder were investigated using X-ray diffractometry, transmission electron microscopy, scanning electron microscopy; differential thermal analysis and Fourier transform infrared spectroscopy. The results showed that CeO<sub>2</sub> with an average particle size of 45 nm is formed. The BET surface area increased to 41m<sup>2</sup>/g, with increasing calcinations to 300 °C; then, it decreased following calcinations at higher temperatures. The particles

---

<sup>†</sup> Corresponding author Tel.: (+98) 21 88011001, fax: +98 21 8005040;  
Email: tabrizi1980@yahoo.com (S.A. Hasanzadeh-Tabrizi)

sintered and agglomerated together after 500 °C. The activation energy for CeO<sub>2</sub> nanocrystallite growth during calcinations was calculated to be about 14.6kJ/mol.

*Keywords:* Ceria nanoparticles; reverse precipitation; Characterization methods.

## 1. Introduction

Ceria (CeO<sub>2</sub>) is a fluorite-structured ceramic material that does not show any known crystallographic change from room temperature up to its melting point (2700 °C).<sup>1</sup> In recent years, nanocrystalline cerium oxide (CeO<sub>2</sub>) particles have been extensively studied owing to their potential uses in many applications, such as UV absorbents and filters<sup>2</sup>, buffer layers with silicon wafer<sup>3</sup>, gas sensors<sup>4</sup>, catalysts in the fuel cell technology<sup>5</sup>, catalytic wet oxidation<sup>6</sup>, engine exhaust catalysts<sup>7</sup>, NO removal<sup>8</sup>, photocatalytic oxidation of water<sup>9</sup>, etc. CeO<sub>2</sub> nanopowders have been reported to be synthesized by different techniques such as: hydrothermal<sup>10</sup>, mechanochemical<sup>11</sup>, sonochemical<sup>12</sup>, combustion synthesis<sup>13</sup>, sol–gel<sup>14</sup>, semi-batch reactor<sup>15</sup>, microemulsion<sup>16</sup> and spray-pyrolysis<sup>17</sup>. Compared with these methods, homogeneous precipitation method is one of the most promising techniques because of the inexpensive starting materials, a simple synthesis process and commonly available apparatus. Although CeO<sub>2</sub> nanoparticles prepared by the precipitation technique have been extensively studied but most of the previous reports were focused on direct precipitation of ceria without using a dispersant.

In the present work, a CeO<sub>2</sub> nanopowder was synthesized via a reverse precipitation method using CeCl<sub>3</sub>·7H<sub>2</sub>O and NH<sub>4</sub>OH as precipitation agent. Sodium dodecyl sulfate (SDS), as a common anionic surfactant, was selected as dispersant to reduce agglomeration.

## 2. Experimental procedure

CeO<sub>2</sub> nanopowder was prepared by a reverse precipitation method using CeCl<sub>3</sub>·7H<sub>2</sub>O (Merck, purity>99.5%), NH<sub>4</sub>OH (Merck, purity> 99%) and SDS (Sigma–Aldrich). CeCl<sub>3</sub>·7H<sub>2</sub>O and SDS were dissolved in deionized water. The molar ratio of Ce<sup>4+</sup> to SDS was 2. The solution was added drop-wise to NH<sub>4</sub>OH while keeping a constant pH value of 8.5 by adding extra-ammonia solution. The resultant synthesis precipitate was washed with deionized water and dried at 80 °C for 24 h. The dried precipitate was calcined for 2 h in a tube furnace at different temperature.

The crystalline structure of the powders was determined by X-ray diffraction (Philips pw 3710) with Cu K $\alpha$  radiation. The average crystallite size (d) of the powder was estimated from the Scherrer equation (Eq. 1):

$$d = \frac{0.9\lambda}{\beta_{sample} \cos(\theta)} \quad (1)$$

where  $\lambda$  is the wavelength,  $\theta$  is the diffraction angle, and  $\beta_{sample}$  is the full-width for the half-maximum (FWHM) intensity peak of the powder. For instrumental correction, the Gaussian–Gaussian relationship (Eq. 2) was used:

$$\beta_{sample}^2 = \beta_{exp}^2 - \beta_{ins}^2 \quad (2)$$

where the measured FWHM of the powder is shown by  $\beta_{\text{exp}}$  and that of the standard sample is indicated by  $\beta_{\text{ins}}$ . Differential thermal analyses (DTA) and thermo gravimetric (TG) were used in the range of 25-1000 °C with a rate of 10°C/min<sup>1</sup> (the STA 1460 equipment). N<sub>2</sub> adsorption-desorption isotherms were determined in a surface analyzer equipment at 77 K. The powder morphology was observed using a Phillips XL30 scanning electron microscope (SEM) and transmission electron microscope (TEM, CM200-FEG- Phillips). Fourier transformation infrared spectroscopy analysis (FTIR) of dried precipitate and calcined powders was carried out in Bruker equipment (Vector-33 model).

### 3. Result and discussion

The synthesis mechanisms may be described by the following reactions. A precipitate is obtained by adding solution to NH<sub>4</sub>OH. The formation of cerium hydroxide occurred after oxidation of Ce<sup>3+</sup> to Ce<sup>4+</sup> in solution at a high pH, leading to  $\text{Ce}^{3+} + \text{H}_2\text{O} \rightarrow \text{Ce}(\text{OH})^{3+} + \text{H}^+ + \text{e}^-$ , with subsequent hydrolysis to Ce(OH)<sub>4</sub> and precipitation. However, oxidation of Ce(OH)<sub>3</sub> also occurs in air at room temperature<sup>18</sup>. Then Ce(OH)<sub>4</sub> converts to CeO<sub>2</sub> with removing the hydroxyl groups (reaction1).



Fig. 1 presents thermogravimetry and differential thermal analysis (TG–DTA) curves of the dried precipitate. The DTA curve shows an endothermic peak at 250 °C which is attributed to evaporation of absorbed water and dehydration of the dried precipitate. TG curve shows an overall weight loss of approximately 10% up to 650 °C and reveals less change at higher temperatures.

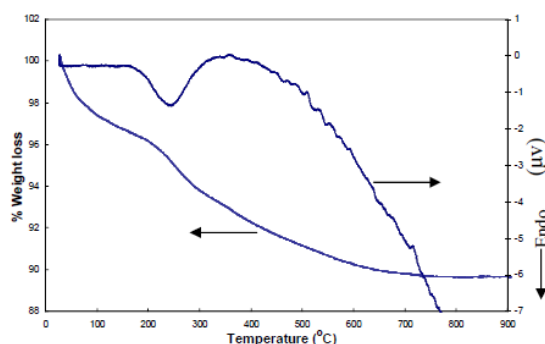


Fig. 1. DTA and TG curves of the dried precipitate.

The X-ray diffraction patterns of the dried precipitate and calcined powders for 2 h at

temperature ranges from 100 to 900 °C are shown in Fig. 2. It is clear that, before heat treatment the precipitate shows broad peaks of CeO<sub>2</sub> nanocrystallites with pure cubic structure. By increasing the heat-treatment temperature to 900 °C, the broadening of CeO<sub>2</sub> peaks decreases which shows growing the CeO<sub>2</sub> nanocrystallites.

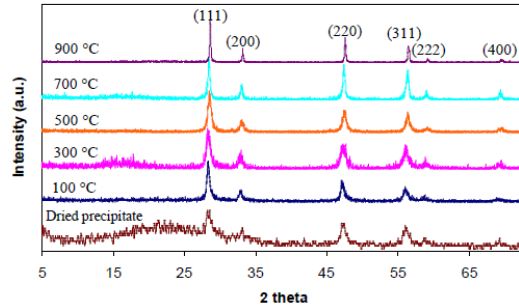


Fig. 2. XRD patterns of as-prepared and heat treated samples at various temperatures for 2 h.

The evolution of crystallite size of the CeO<sub>2</sub> powder during calcinations has been investigated, and the results obtained from X-ray line-broadening of the (111) peak are summarized in Fig. 3. As can be seen, crystallite size decreases from 13.4 to 11 nm with increasing the calcinations temperature to 300 °C. This decrease results most probably from broadening of diffraction peaks due to destabilization of the low-temperature cubic phases, rather than from actual shrinking of crystallites.<sup>19</sup> By increasing the temperature more than 300 °C, crystallite size increases. Increasing of crystallite size is attributed to typical effect of temperature on crystal growth. For instance, Li et al.<sup>20</sup> reported that the crystallite size of CeO<sub>2</sub> shows exponential dependence on the calcinations temperature, indicating that crystallite growth is diffusion related.

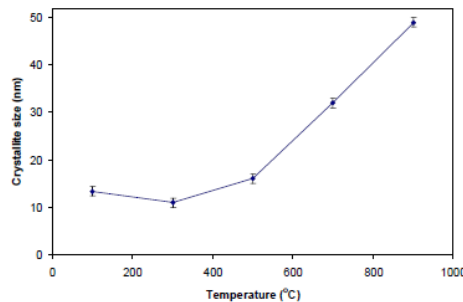


Fig. 3. Effect of calcination temperature on Crystallite size of CeO<sub>2</sub>.

In addition, it is obvious that the nanocrystallites grow slowly up to 500 °C and then they grow rapidly. In the case of low calcinations temperature (300 < T < 500 °C), the porosity is quite high and the pores are interconnected to maintain smaller crystal sizes.<sup>21</sup> For the specimens calcined at higher temperatures (>500 °C), continuous grain boundary networks have been formed due to the bridging of fine particles to increase the crystal sizes.

Straight line of  $\ln(D)$  against  $1/T$  is plotted in Fig. 4 according to the Scott equation,

given below on the assumption that the nanocrystallite growth is homogeneous<sup>22</sup>, which approximately describes the nanocrystallite growth during annealing:

$$D = C \exp\left(-\frac{E}{RT}\right) \quad (3)$$

Where D is the XRD crystal size, C is the constant, E is the activation energy for nanocrystallite growth, R is the ideal gas constant and T is the absolute temperature of heat treatment. The activation energy for CeO<sub>2</sub> nanocrystallite growth during calcinations was calculated to be about 14.6kJ/mol. It can be considered that the crystallite grows by means of an interfacial reaction<sup>23</sup>.

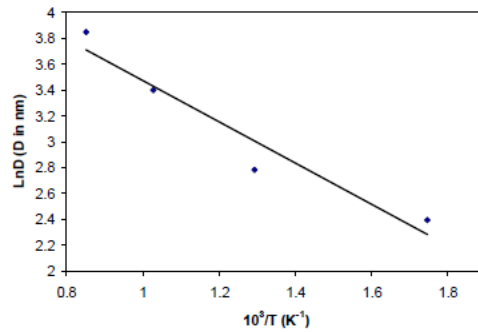


Fig. 4. Plot of Ln (D) against 1/T for the equation  $D = C \exp(-E/RT)$

The effect of the calcination temperature on the surface area is shown in Fig. 5. The surface area increases at 300 °C (41 m<sup>2</sup>/g); then, it decreases when the temperature becomes higher. Increasing surface area is due to rapid decomposition of the precipitate accompanied by the appearance of considerable stresses, which leads to decomposition of the particles. With increasing temperature from 300 to 500 °C, the surface area decreases due to the grain growth. By increasing the temperature above 500 °C, surface diffusion can be activated and it can cause sintering and formation of necks between particles. Therefore surface area reduces with higher rate above 500 °C.

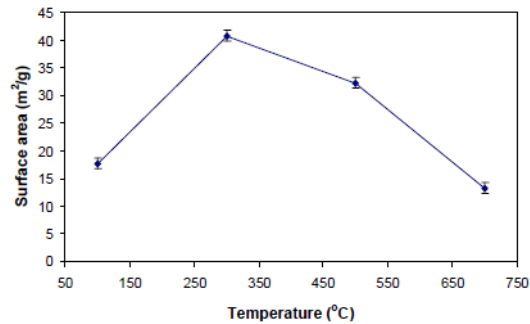


Fig. 5. Effect of calcination temperature on surface area.

Fig. 6 shows the TEM Micrograph of powder calcined at 300 °C. As can be seen the size of particles is about 45 nm. The particle size in this figure is larger than the crystallite sizes obtained via X-ray line-broadening analysis (Fig. 6). These obvious discrepancies indicate that the particles are polycrystalline. In addition TEM micrograph shows most of the particles are spherical in shape. Considering that the CeO<sub>2</sub> has been synthesized by wet soft chemistry, the uniform size and shape are achieved. Cabus-Llaurado et al.<sup>24</sup> synthesized a CeO<sub>2</sub> nanopowder by a precipitation method using CeCl<sub>3</sub>·7H<sub>2</sub>O and (NH<sub>4</sub>)<sub>2</sub>CO<sub>3</sub> as precipitation agent and showed, synthesized nanopowders have a layered structure with high surface area. Therefore it can be concluded that the precipitation agent have strong effect on morphology of resultant powder. In addition Chen et al.<sup>25</sup> found that, calcinations atmosphere plays an important role on the size and shape of resulting particles in precipitation method.

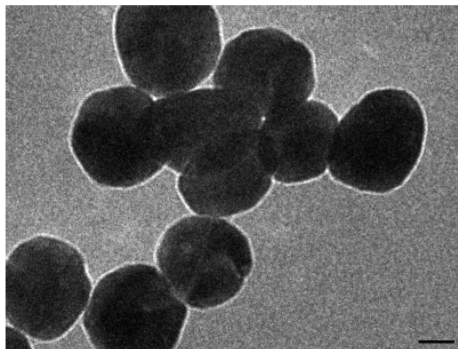


Fig. 6. TEM image of the nanopowders heat treated at 300°C (bar = 20 nm).

Fig. 7 presents the SEM images of the powder heat treated at 500 and 700 °C. As can be seen there are some individual particles in the powders heat-treated at 500 °C. In addition some small agglomerates exist in the powders which are attributed to uncontrolled coagulation during precipitation. Fig. 7 (b) shows that the particles cling together and form larger agglomerated structures. By increasing the temperature above 500 °C, the mechanism that can be activated is surface diffusion, which leads to neck formation and further agglomeration. It shows that the synthesized powder starts to sinter at low

temperatures. This powder can be used as raw material for fabrication of bulk ceria.

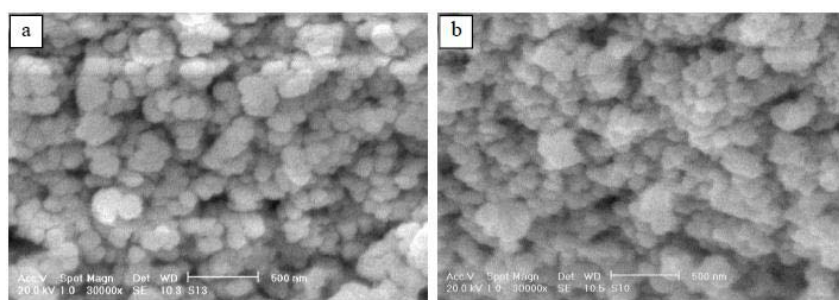


Fig. 7. SEM images of the powders heat treated at different temperatures: (a) 500 °C (b) 700 °C.

Fig. 8 shows the FTIR spectra of the CeO<sub>2</sub> nanopowder heat-treated at various temperatures for 2h. The absorption broad peak at 3000-3600 cm<sup>-1</sup> and absorption peak at around 1620 cm<sup>-1</sup> maybe attributed to the O-H vibration of water. The two absorption peaks become weaker by increasing the heat-treatment temperature. The broad band below 700 cm<sup>-1</sup> is due to the envelope of the phonon band of the metal oxide network. By increasing the temperature hydroxyl groups are decomposed in the precipitate and only Ce-O bands are remained.

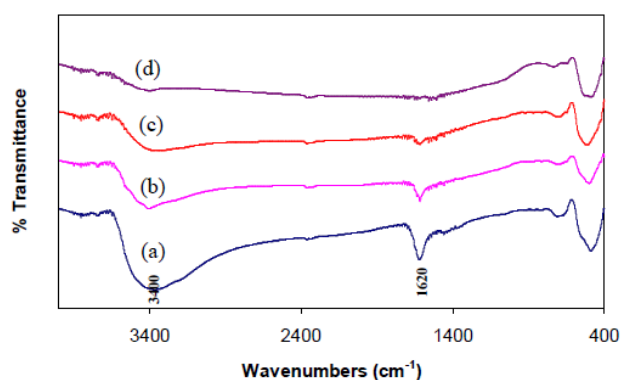


Fig. 8. IR spectra of CeO<sub>2</sub> precipitate at various temperature: (a) 100 °C (b) 300°C (c) 500 °C (d) 700°C.

#### 4. Conclusions

In the present study a CeO<sub>2</sub> nanopowder was synthesized by a reverse precipitation method using CeCl<sub>3</sub>·7H<sub>2</sub>O, NH<sub>4</sub>OH and SDS as raw materials. The findings can be

summarized as follow:

1- CeO<sub>2</sub> with an average particle size of 45 nm was formed. The morphology of the prepared powder is sphere-like with a narrow size distribution. The total weight loss of 10% appears in the specimens after heat treatment due to removing of volatile components.

2- The activation energy for CeO<sub>2</sub> nanocrystallite growth during calcination was calculated to be about 14.6kJ/mol. By increasing the temperature above 500 °C, the particles clung together and formed larger agglomerates.

3- The BET surface area increased to 41 m<sup>2</sup>/g with increasing calcinations temperature to 300 °C; then, it decreased following calcination at higher temperatures. The surface area reduced with higher rate above 500 °C.

## References

1. J. Li, T. Ikegami, T. Mori, *Acta Materialia*, 52, 2221–2228 (2004).
2. S. Tsunekawa, T. Fukuda, A. Kasuya, *Journal of Applied Physic*, 8, 1318–1321 (2000).
3. J. Tashiro, A. Sasaki, S. Akiba, S. Satoh, T. Watanabe, H. Funakubo, M. Yoshimoto, *Thin Solid Films*, 415, 272–275 (2002).
4. F.H. Garzon, R. Mukundan, E.L. Brosha, *Solid State Ionics*, 136-137, 633–638 (2000).
5. S. Logothetidis, O. Patsalas, C. Charitidis, *Journal of Materials Science and Engineering C*, 23, 803–806 (2003).
6. F. Larachi, J. Pierre, A. Adnot, A. Bernis, *Journal of Applied Surface Science*, 195, 236–250 (2002).
7. M.T. Dario, A. Bachiorelli, *Journal of Ceramic International*, 25, 511– 516 (1999).
8. R. DiMonte, P. Fornasiero, M. Graziani, J. Kaspar, *Journal of Alloys and Compound*, 277, 877–885 (1998).
9. G.R. Bamwenda, H. Arakawa, *Journal of Molecular Catalysis A*, 161, 105–113 (2000).
10. Y.C. Zhou, M.N. Rahaman, *Journal of Material Resistance*, 8, 1680-1686 (1993).
11. Y. X. Li, W. F. Chen, X. Z. Zhou, *Materials Letters*, 59, 48-52 (2005).
12. J. C. Yu, L. Zhang, J. Lin, *Colloidal Interface Science*, 260, 240-243 (2003).
13. W. Chen, F. Li, J. Yu, *Materials Letters*, 60, 57-62 (2006).
14. M. Alifanti, B. Baps, N. Blangenois, *Chemical Material*, 15, 395-403 (2003).
15. X. D. Zhou, W. Huebner, H. U. Anderson, *Chemical Material*, 15, 378-382 (2003).
16. J. S. Lee, S. C. Choi, *Materials Letters*, 59, 395-398 (2005).
17. T. Yoshioka, K. Dosaka, T. Sato, *Journal of Materials Science Letters*, 11, 51-55 (1992).
18. B. Djuricic, S. Pickering, *Journal of the European Ceramic Society*, 19, 1925–1934 (1999).
19. M. Karbowski, A. Mech, L. Kepiński, W. Mielcarek, S. Hubert, *Journal of Alloys and Compound*, 400, 67–75 (2005).
20. J. G. Li, T. Ikegami, J. H. Lee, T. Mori, *Acta materialia*, 49, 419-426 (2001).
21. T. Lai, Y. Shu, G. Huang, C. Lee, C. Wang, *Journal of Alloys and Compound*, 450, 318–322 (2008).
22. M.G. Scott, *Amorphous Metallic Alloys* Butterworths, London, 1983, p. 151.
23. H. Yang, C. Huang, A. Tang, X. Zhang, W. Yang, *Materials Resistance Bulletin*, 40, 1690–1695 (2005).
24. M. C. Cabus-Llaurado, Y. Cesteros, F. Medina, P. Salagre, J. E. Sueiras, *Microporous and Mesoporous Materials*, 100, 167-172 (2007).
25. H. Chen, H. Chang, *Solid State Communication*, 133, 593-598 (2005).